Sustainable Cities and Society 80 (2022) 103746

Contents lists available at ScienceDirect

Sustainable Cities and Society

journal homepage: www.elsevier.com/locate/scs

Urban scale ventilation analysis based on neighborhood normalized current model

Peng Xie [a], Jun Yang [b,c,*], Wei Sun [d,**], Xiangming Xiao [e], Jianhong Cecilia Xia [f]

[a] School of Civil Architectural Engineering, Shandong University of Technology, Zibo, Shandong 255000, China
[b] Human Settlements Research' Lab, Jangho Architecture College, Northeastern University, Shenyang, China
[c] Human Settlements Research Center, Liaoning Normal University, Dalian, Liaoning 116029, China
[d] Nanjing Institute of Geography and Limnology, Key Laboratory of Watershed Geographic Sciences, Chinese Academy of Sciences, Nanjing 210008, China
[e] Department of Microbiology and Plant Biology, Center for Spatial Analysis, University of Oklahoma, Norman, OK 73019, USA
[f] School of Earth and Planetary Sciences (EPS), Curtin University, Perth 65630, Australia

ARTICLE INFO

Keywords:
Urban ventilation
Morphological analysis
Hydrodynamics analysis
Heat island effect
Wuhan

ABSTRACT

With increasing urbanization, the urban heat island (UHI) effect has become a critical urban environmental problem. Many factors affect the formation of UHIs, and urban canopy ventilation is considered a crucial method for reducing the UHI effect. This study proposed an improved ventilation corridor (VC) identification method known as the neighborhood normalized current model (NN-CM). This method uses neighborhood normalization to improve VC identification based on circuit theory. Considering Wuhan, China, as the research area using three-dimensional building data, urban ventilation environment simulation experiments under different wind directions were conducted on a 100 m grid. The results were compared, and computation fluid dynamics (CFD) analysis was used to verify the proposed method. Compared with the original VC analysis method based on circuit theory, the proposed method reduced the subjectivity of the analysis results. Further, compared with other methods, the new method was advantageous in analysis result coverage, dynamic wind direction simulation, and data throughput. The CFD verification confirmed that the NN-CM exhibits high reliability.

1. Introduction

Urbanization and the subsequent expansion of impervious areas exacerbate the urban heat island (UHI) effect, which is characterized by the temperature difference between a central urban area and the surrounding rural area (Gu, Fang, Qian, Sun, & Wang, 2020; Kim, Gu, & Kim, 2018; Mostafavi, Tahsildoost, & Zomorodian, 2021; Yang et al., 2020). The UHI effect has become one of the most significant characteristics of urban climate (Ren et al., 2022). With increasing urbanization, there have been reports of UHIs worldwide (Yang et al., 2019; Zou et al., 2021). UHIs change the urban thermal environment and lead to a series of environmental problems by affecting the regional climate, urban hydrology, air quality, physical and chemical properties of the urban soil, and behavior of urban organisms. Several studies have demonstrated that UHIs are closely related to various factors, such as human-related heat release, underlying surface properties and structure, vegetation cover, population density, and weather conditions (Chun & Guldmann, 2018; Lee & Mak, 2021, 2021; Qiao et al., 2019; Ren, Cai, Li, Shi, & See, 2020). Of these, urban ventilation corridors (VCs) formed according to the underlying surface properties and structures can substantially reduce UHIs (Du & Mak, 2018; Ren et al., 2018; Xie, Liu, Liu, & Liu, 2020; Yang et al., 2019; Zhang, Zhan, & Lan, 2018).

Urban canopy airflow is a critical factor in controlling the formation of UHIs (Gautam, Rong, Zhang, & Abkar, 2019; Yang et al., 2020). Dense building areas cannot easily release heat energy into the atmosphere due to the lack of open spaces. High-rise buildings block airflow and reduce its cooling effect, isolating hot air in the canyon. In addition, when solar radiation reaches the building surface, it is absorbed into the wall. Consequently, the temperature of the air surrounding these walls increases (Yang et al., 2021). Many experts have incorporated VCs into their urban planning strategy to mitigate UHI, thereby promoting further research on this topic (Yang, Yang, Sun, Jin, & Xiao, 2021; Yuan, Norford, Britter, & Ng, 2016).

VC simulation methods can be divided into two categories:

* Corresponding author at: Human Settlements Research' Lab, Jangho Architecture College, Northeastern University, Shenyang, China.
** Corresponding author.
E-mail addresses: xiepenggis@163.com (P. Xie), yangjun8@mail.neu.edu.cn (J. Yang), wsun@niglas.ac.cn (W. Sun).

https://doi.org/10.1016/j.scs.2022.103746
Received 14 October 2021; Received in revised form 4 January 2022; Accepted 29 January 2022
Available online 31 January 2022
2210-6707/

hydrodynamics-based and morphology-based methods. Methods based on hydrodynamics include wind tunnel experiments and computational fluid dynamics (CFD) (He et al., 2019; He, Tablada, & Hien, 2019, 2018). These methods can provide accurate wind speed information. Due to their high experimental cost, hydrodynamics-based methods are suitable for accurate building-scale simulation and analysis, such as the ventilation simulation of a single building or community. In contrast, methods based on morphological analysis are widely used in urban scale VC analysis owing to their low computational cost. Morphological analysis includes calculations of the urban canopy morphological index, such as the front area index (FAI) and sky view factor (Gál & Unger, 2009; Lan & Zhan, 2017; Yang, Qian, & Lau, 2013). Based on the morphological index, the spatial distribution of VCs can be analyzed using spatial analysis methods, such as rule-based, least-cost path (LCP), and current theory-based methods. Rule-based methods establish a linear relationship between the morphological index and CFD-simulated wind speed to identify VCs as spatially continuous low-value regions (Gu et al., 2020; Wicht, Wicht, & Osińska-Skotak, 2017). These methods are user-friendly and widely used. Due to the lack of a wind direction analysis mechanism, the distribution characteristics of VCs under multiple wind directions have not yet been determined. The LCP-based methods assume that the airflow is in the direction with the lowest wind resistance; this path with the least accumulated wind resistance is then identified as the VC (Chen, Lu, & Yu, 2017; Qiao et al., 2019, 2017; Wong, Nichol, To, & Wang, 2010). These methods can effectively identify the primary VCs; however, the analysis results cannot cover the entire study area or effectively express the VC shapes.

The circuit theory-based method, recently proposed by Xie, Yang, Wang, Liu, & Liu (2020), performs multi-wind direction simulation and presents full-coverage results, resolving the shortcomings of the aforementioned methods. This method assumes that when the airflow meets a branch formed by multiple buildings, it is distributed according to the inverse proportion of the wind resistance of each branch. The resulting flow reflects the ventilation capacity, and the shapes of the VCs can be determined by flow reclassification. The threshold used for reclassification directly affects the distribution of VCs; therefore, this method demonstrates a strong subjectivity impact.

This study applied an improved current theory-based method called the neighborhood normalized current model (NN—CM) that transforms the current density into a value relative to the neighborhood average by integrating the neighborhood and current analyses. Because the analysis results range from −1 to 1, it can be used to identify whether the area is beneficial to ventilation according to whether the value is greater than 0. The NN—CM method utilizes the neighborhood analysis method to conduct a secondary analysis of the flow data. By comparing the relative relationship between the absolute and average airflow values in the neighborhood, the absolute value of the airflow is transformed into the relative airflow value of [−1, 1]. VCs were simulated in this study using three-dimensional building data and NN—CM. In particular, the study aimed to (1) calculate the relative current and (2) verify the NN—CM using a multi-method-based approach.

2. Methods

Fig. 1 shows the methodological framework of NN—CM. This model included two input datasets (3D building data and background wind data) and one output dataset (urban scale ventilation analysis results). There are three modules in NN—CM: front ventilation index module, current module, and neighborhood normalization module. Each module has been described comprehensively in the paper.

2.1. Front ventilation index

The FAI is defined as the ratio of the total windward projected area of buildings to the regional area. It has been widely used to measure the ventilation resistance of urban canopies. The greater the FAI value, the greater the roughness of the urban canopy and wind resistance. The equation is as follows:

$$\lambda_f = \frac{A_f}{A_p} \tag{1}$$

where A_f represents the projected area of the windward side of the building, and A_p represents the regional planar area. Based on the FAI, the front ventilation index (FVI) was proposed to express the ventilation capacity (Fig. 2). The equation is as follows:

$$G_h = \left(\frac{A_h - A_f}{A_p}\right) \tag{2}$$

where A_h represents the projected area of the windward side of the building with height h, A_f represents the projected area windward side of the building in the same area, and A_p represents the planar area of the region.

2.2. Current module

Circuit theory can be used to analyze VC problems (McRae, Dickson, Keitt, & Shah, 2008; Xie et al., 2020). Fig. 3 displays a ventilation network composed of connecting edges and nodes. The edges represent functional connectivity, and their weights represent the ventilation capacity of the path. When applying the circuit theory to solve the connectivity problem of the ventilation network, conductance can be used to represent the ventilation capacity of the corridor (Fig. 3). This method can effectively reveal the ventilation capacity between two points under

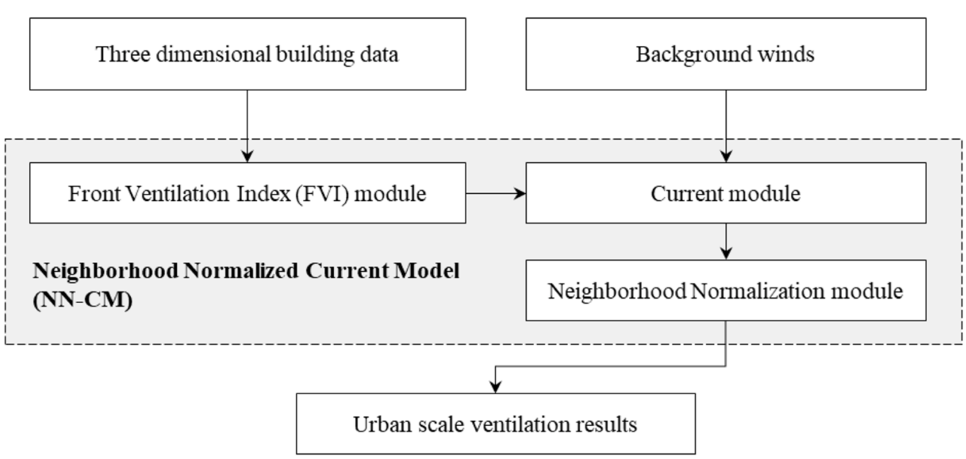

Fig. 1. Proposed methodological framework for mapping urban scale ventilation.

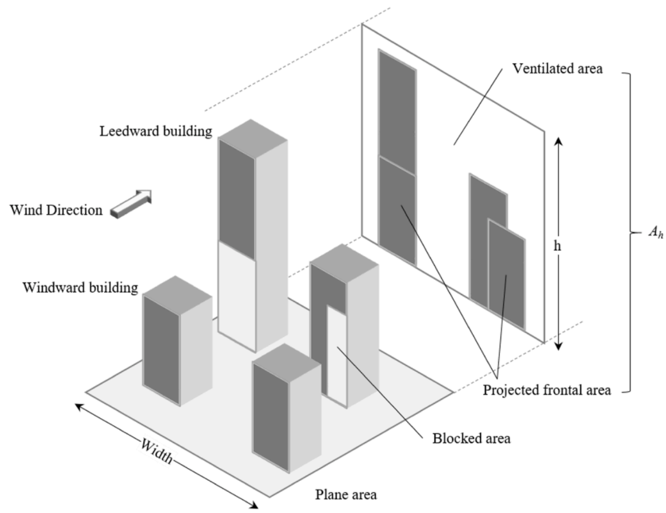

Fig. 2. Front ventilation index (FVI) definition.

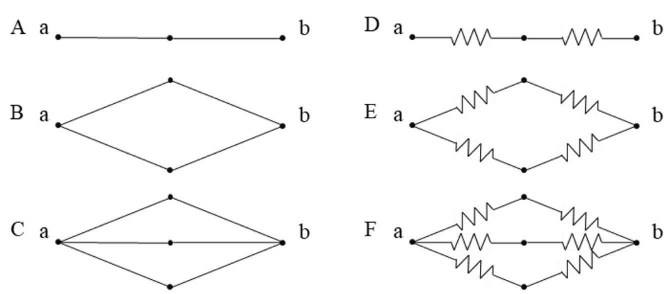

Fig. 3. Differences in node connectivity between single and multiple paths. The weight of each edge is 1 in A, B, and C. According to the traditional LCP method, the cost distance between nodes a and b in A, B, and C is 2. In D, E, and F, the edges are replaced with resistors with unit conductivity values, and the relative resistance values between nodes a and b are 2, 1, and 2/3, respectively. (Figure modified from McRae and Dickson, 2008).

the condition of multiple paths. The following sections provide explanations of the conductance, current, and voltage.

2.2.1. Current

Unlike the LCP method, which assumes that the path with the least ventilation resistance is the VC, the current theory-based method assumes that the flow is distributed according to the branch ventilation capacity when the airflow meets the branch. For example, consider an undivided air mass μ with a unit mass. When it passes through an intersection, the probability of selecting each branch is directly proportional to the branch ventilation capacity. The current value represents the probability of μ passing through each branch, and the conductivity value represents the branch ventilation capacity. The branch ventilation probability, as displayed in Fig. 4 can be expressed using the following equation:

$$\frac{I_{bc}}{I_{bd}} = \frac{G_{bc}}{G_{bd}} \tag{3}$$

where I_{bc} and I_{bd} represent the currents passing through the BC and BD branches, and G_{bc} and G_{bd} represent the conductance of branches BC and BD, respectively. In the VC analysis, I_{bc} and I_{bd} represent the airflows of branches BC and BD, respectively. The currents can be used to identify the tuyeres. The higher the flow through a node or branch, greater is the contribution of the node or branch to the ventilation. Blocking the node or branch substantially negatively impacts the ventilation. As illustrated in Fig. 4, all currents pass through node b. Blocking node b or linking

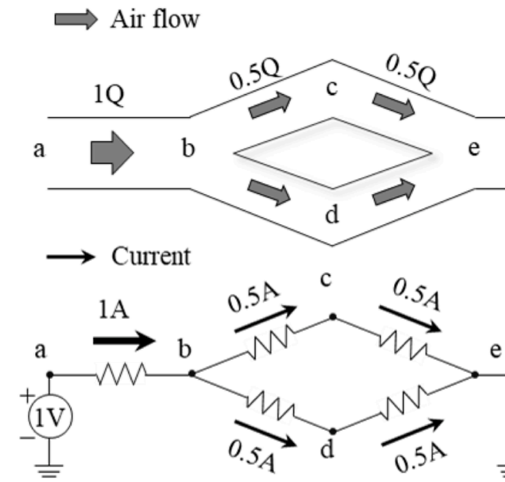

Fig. 4. Interpretations of current, voltage, and resistance. (Figure based on McRae and Dickson, 2008) .

nodes a–b cuts off the connectivity between nodes a and e, while blocking node c reduces the number of available paths but maintains connectivity.

2.2.2. Conductance

The conductance value represents the current-carrying capacity of the resistor. In this study, the FVI was used as the conductance to represent the airflow passing effect of the VC in an urban canopy. The larger the FVI, the easier it is for the air to pass, and vice versa. The calculation of FVI is described in Section 2.1.

2.2.3. Voltage

In the ventilation simulation, the primary function of the voltage is to configure the background wind direction. As displayed in Fig. 4, node a has high voltage, whereas node e has low voltage. A stable current forms between nodes a and e through the link between resistors. Correspondingly, there is high air pressure at node a and low air pressure at node e, forming airflow between nodes a and e. If the voltage at node a is set to 1 V, and the voltage at node e is set to 0, the voltage measured at any node in the figure can be used to represent the probability of μ beginning from node a and arriving at the node first.

2.3. Neighborhood normalization module

The original current values were all greater than 0. Although the VCs can be identified using current reclassification, there is great subjectivity when selecting the reclassification threshold. This study presented an NN-MC method. Using a neighborhood normalization module, the method identified the areas conducive to ventilation as positive values and those hindering ventilation as negative values (Fig. 5). The equation is as follows:

$$I_i' = I_i - \sum_j^{\Omega} I_j \cdot w_j \tag{4}$$

$$I_i^* = \begin{cases} \dfrac{I_i'}{Max(I')} & (I_i' \geq 0) \\ -\dfrac{I_i'}{Min(I')} & (I_i' < 0) \end{cases} \tag{5}$$

where I_i^* represents the modified current value at location i, I' represents the set of I_i', I_i represents the original current value at location i calculated by the method proposed by Xie et al. (2020), Ω represents a neighborhood near location i, I_j represents the current value at location j

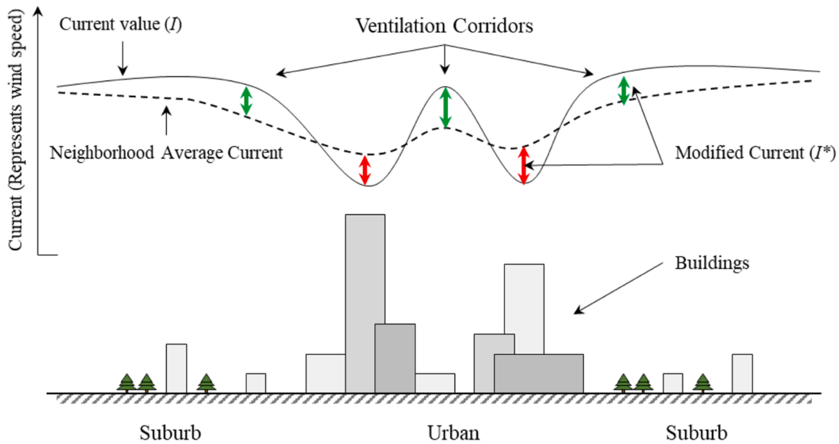

Fig. 5. Interpretations of modified current .

within Ω, and w_j represents the weight of I_j. In the following case study, w_j is equal to the reciprocal of the number of grid cells in Ω.

When $I_i^* > 0$, location i is conducive to ventilation, when $I_i^* < 0$, location i is unconducive to ventilation, and when I_i^* is near 0, the ventilation at location i is near the background value.

2.4. *Case study*

2.4.1. *Study area*

Wuhan (between 113.7E–115.0E and 29.9N–31.3 N) is the capital city of Hubei Province in central China (Fig. 6). Wuhan receives abundant rainfall and sunshine through the southeast monsoon in summer and the northwest wind in winter. As the core development city of central China, the built-up area in Wuhan has expanded rapidly. In the last few years, the UHI area in midsummer accounted for more than 25% of the total area of Wuhan. Urban ventilation has increasingly become one of the primary hindrances to sustainable urban development in this area. The land use, road, and three-dimensional data of the buildings for 2015 were provided by the Wuhan Planning Bureau.

2.4.2. *Calculation process*

To determine the height (h) in the ventilation index (G_h), we assumed that the number of floors in high-rise buildings in Wuhan was approximately 33, and the number of super high-rise buildings was small. Setting $h = 100$ m, 99.9% of the building area was included in the study. The study area formed a closed circuit. In this study, a circular simulation area with the city center as the circle center and a radius of 40 km was adopted to ensure a large buffer area between the study area boundary and built-up area. The default FVI value of the buffer area was 1. Starting from 0°, inlets and outlets in 16 directions were set at

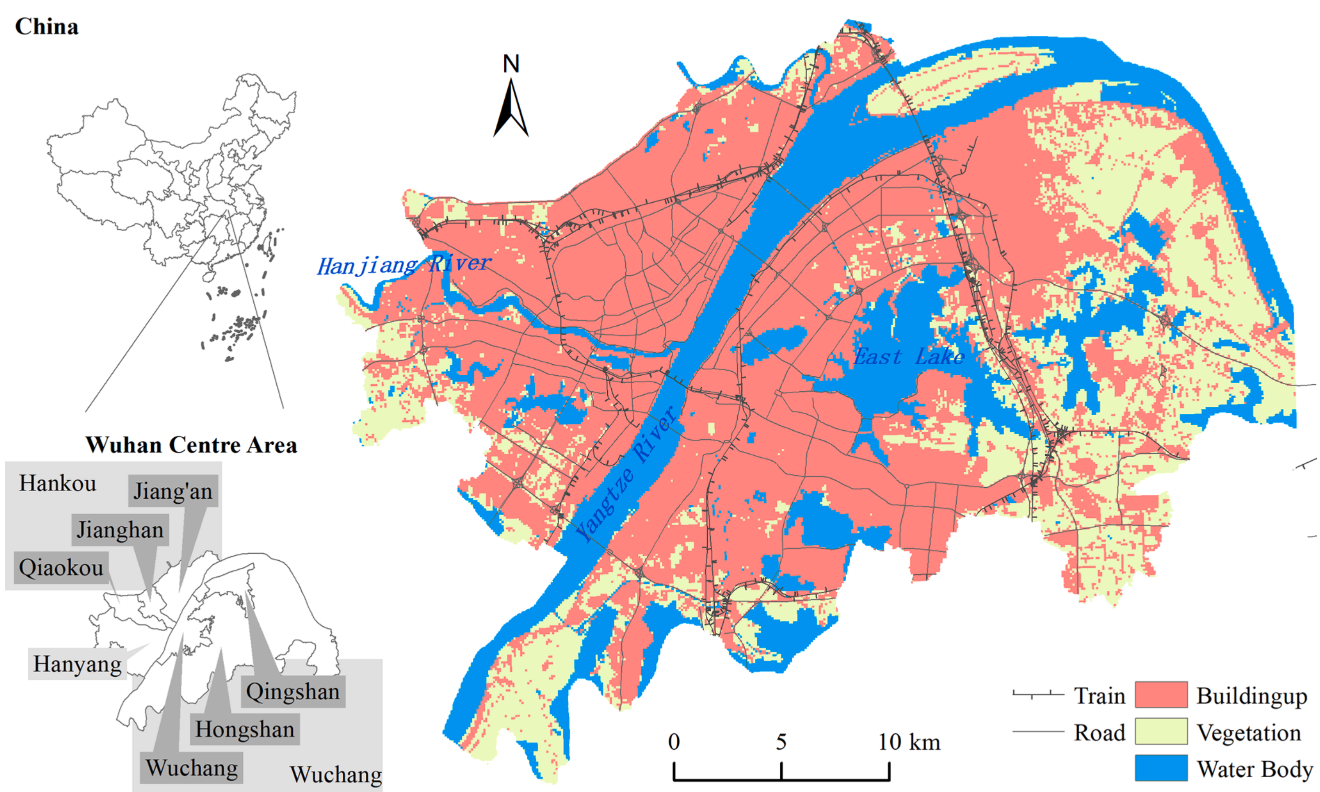

Fig. 6. Location of the study area. The Yangtze River and Hanjiang River meet in the city, dividing Wuhan into Hankou (including Qiaokou, Jianghan, and Jiang'an), Wuchang (including Qingshan, Hongshan, and Wuchang), and Hanyang.

intervals of 22.5° (Fig. 7).

To implement the circuit algorithm, the ventilation index grid was transformed into a graphical structure. When the grid size is 100 m, ventilation characteristics can be sufficiently explored at the urban scale (Hsieh & Huang, 2016; Wong & Nichol, 2013; Wong et al., 2010; Yuan, Ren, & Ng, 2014). Therefore, the grid size was set to 100 m in this study. When the grid data were converted to graphical data, a grid cell was considered a node, the adjacent nodes were connected by resistance, and the conductance value of the resistance was equal to the average FVI value of the linked nodes. Adjacent cells with zero resistance (infinite conductance) were merged into one node. The gray grids in Fig. 8 represent the conductance. Following these steps, a grid with 16 cells was transformed into a circuit with 13 nodes and 22 resistors.

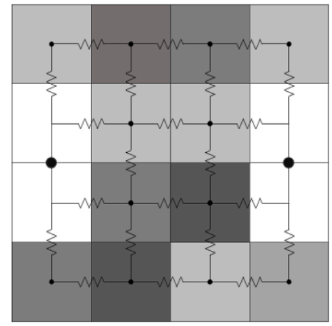

Fig. 8. Basic example represented in both grid and circuit forms. (Figure based on McRae and Dickson, 2008) .

3. Results

3.1. Distribution of FVI

Fig. 9 displays the spatial distributions of the buildings and FVI in a 100 m grid in the central urban area of Wuhan. There were 101,328 buildings in the study area (Table 1). All buildings were divided into four classes: low, medium, high, and super-high, according to the thresholds of <10 m, 10–24 m, 24–100 m, and >100 m, respectively. The proportions of each class were 56.96%, 33.38%, 9.54%, and 0.12%, respectively.

The FVI and building height are generally negatively correlated, and the FVI spatial differentiation was apparent. The FVI exhibited a decreasing trend from the urban center to the periphery, excluding the water surface area. The average building height of the entire area was 14.3 m, and the average FVI of the grid was 0.846. The FVI of Hanyang was superior to that of the other districts, with an average FVI of 0.877 and an average building height of 13.7 m. This was primarily because this area experienced a shorter development period. On one hand, there are many low buildings in this area. On the other hand, ventilation factors have been considered in the developmental planning of high-rise buildings in the area, with sufficient VCs between high-rise building areas in Hanyang. Hankou (Qiaokou District, Jianghan District, and Jiang'an District) is one of the oldest urban areas of Wuhan, with the longest development history and highest development intensity. The ventilation in this area is worse than that in other areas. The average FVI in Hankou is 0.823, and the average building height is 15.9 m. The ventilation in Wuchang District is similar to that in Hankou. This area is near the urban center and has a long development history. The buildings in this area are of mixed height classes. The average FVI was 0.838, and the average building height was 13.36 m. Qingshan District is a crucial heavy industrial base, with many low-level factory buildings and medium-level residential buildings. The average wind FVI was 0.886 in the district, and the average building height was 11.8 m. Hongshan District is a key new urban development area of Wuhan, with an average building height of 13.9 m and an average FVI of 0.856.

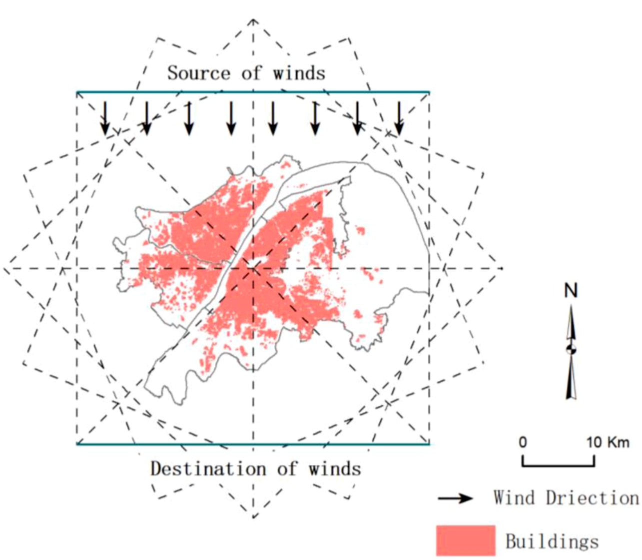

Fig. 7. Inlets and outlets of study area.

3.2. Distribution of VCs

Fig. 10 displays the distribution of urban canopy VCs under 16 wind directions in a 100 m grid in the central urban area of Wuhan, which adopts a circular neighborhood with a radius of 1 km. The continuous blue zones in Fig. 10 represent critical VCs. The VCs exhibited different distribution patterns under different wind directions. Conducive and unconducive ventilation areas were both distributed in long striped shapes, and the directions were consistent with the background wind direction. Table 2 shows the area and its proportion of the conducive ventilation area under different wind directions. As shown in the table, the proportion of conducive ventilation area in Wuchang was better than others (81.75%–84.46%). This was due to the large area of East Lake and suburbs, which promoted ventilation in the area. The worst was in Hankou (64.33%–67.95%), mainly because there were few natural open spaces in this area and the building density was higher than in other areas. From the perspective of different wind directions, the proportion of conducive ventilation area was larger in the NE–SW and SE–NW directions mainly because the Yangtze River passed along the NE–SW direction, and the East Lake, Sha Lake, Han River, and main roads formed the VC framework in the SE–NW direction.

3.3. Comparison of different methods

Fig. 11 compares the Hankou area (Qiaokou, Jiang'an, and Jianghan) results using various methods. The NN—CM, original current model, and LCP model consist of the extraction results under the EN background wind direction. In contrast, the results of the rule-based model were derived from Zou et al. [36] because of similar study area and study time. The VCs identified using various methods were sufficiently consistent.

Fig. 11d shows that the LCP model only locates some of the primary VCs, and the analysis results did not cover the entire area. The rule-based model did not sufficiently reflect the VC pattern under different wind directions. Further, the results based on the original current model and NN—CM were similar. Both models could generate the analysis results covering the entire area in different wind direction environments. The difference was that the value range of the original current model was greater than 0, implying high subjectivity of the division of the VCs. In contrast, the result range of NN—CM was [− 1, 1]. When the value was greater than 0, the area promoted ventilation, and when the value was less than 0, the area hindered ventilation.

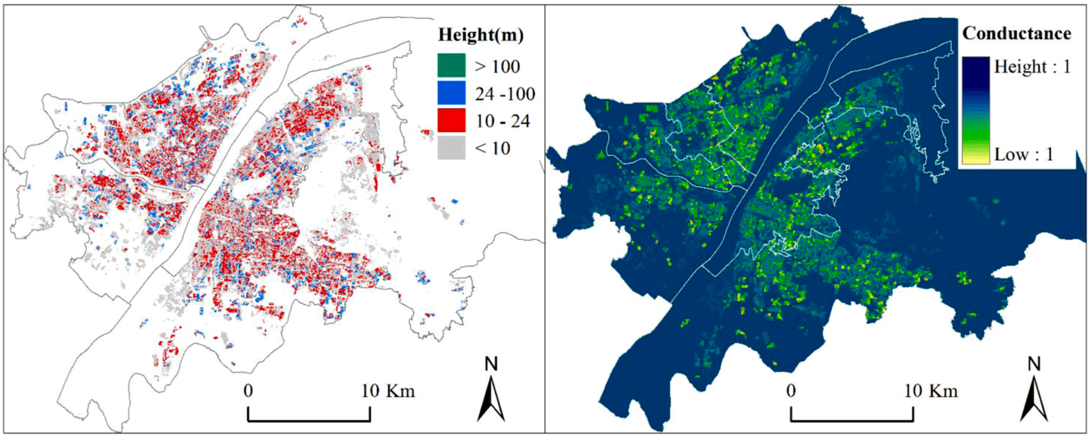

Fig. 9. Spatial distributions of buildings and front ventilation index (FVI).

Table 1
Height of buildings in study area.

Height (m)	Number	Percentage of all buildings (%)	Building area (km^2)	Percentage of total building area (%)
$H \leq 10$	57,720	56.96	32.14	48.91
$10 < H \leq 24$	33,825	33.38	25.28	38.46
$24 < H \leq 100$	9663	9.54	8.20	12.48
$100 < H$	120	0.12	0.10	0.15

3.4. Method validation

To verify the accuracy of the proposed method, a comparative test was performed using CFD (Fig. 12). Due to the operational efficiency of the CFD analysis, we selected a test area constituting a large residential community to the north of the study area. The CFD experiment was conducted using PHOENICS software, and the three-dimensional space of the test area was divided into 10 resolution grids. Air inlets and outlets were set on the N and S sides of the test area to simulate the E wind direction. Because the proposed method used the 100 m grid data, a regional statistical method was used to obtain the average value of the CFD wind speed simulation results in a 100 m grid to compare the results. The geographically weighted regression analysis tool provided by ArcGIS 10.2 was used to analyze the correlation between the CFD-simulated wind speed (v^*) and NN-MC result (modified current I^*). A Gaussian kernel with a 100 m bandwidth was used in the geographic weighted regression analysis. The results demonstrated that the R^2 value was 0.946, and the adjusted R^2 value was 0.858. The verification results illustrated that the proposed method was highly reliable.

4. Discussion

This study improved the analysis method of an urban VC based on the circuit theory to reduce subjectivity. The spatial distribution of the modified current was produced using neighborhood normalization technology, and the original current value was transformed into $[-1, 1]$. The promotion/blocking effect on ventilation could be objectively evaluated according to the sign of the modified current. The advantages, disadvantages, applicable scenarios, and potentiality of this method are discussed in this section.

4.1. Advantages

The results of the proposed model (NN—CM) showed improvement compared to those of the current theory-based method. Compared with other VC analysis methods, the proposed method has the following advantages. (1) Compared with the wind tunnel and CFD methods, the proposed method can process larger amounts of data and is more suitable for urban scale VC simulation. (2) Compared with the LCP-based method, the results of the proposed method can cover the entire study area, as opposed to only covering a portion of it, and provide morphological details of VCs. (3) Compared with the rule-based method, NN—CM can better simulate the characteristics of VCs under different wind directions. (4) Compared with the original method based on the current theory and proposed by Xie et al. (2020), the proposed method can reduce the subjective influence of the current value reclassification.

4.2. Applicable scenarios

The method proposed in this paper can identify VCs with different wind directions at urban scale. It has great potential applications in urban planning as follows: (1) It can intuitively understand the urban ventilation condition. This method can be used to identify conducive and unconducive areas to ventilation. The identification of these areas can maximize the use of urban environmental improvement funds. (2) This method can provide decision support for urban VC planning. Planners can select some of the ventilation conducive areas as data support for urban VC planning. These selected areas usually have the characteristics of large width, long length, and wide coverage. (3) This method provides a predictable analysis approach for urban form development, especially when the amount of data is too large to implement the CFD method. Further, urban scale ventilation verification can be conducted for various design schemes. The optimal planning scheme can be selected from these schemes, which can improve the urban ecological environment. (4) The proposed method can be used to compare the morphological differences of VCs between cities, which helps explore the formulation of sustainable urban development strategies.

4.3. Ventilation patterns in Wuhan

This study provided a simple method for urban planners to understand the urban ventilation environment. The main findings are as follows: (1) The central urban area of Wuhan covers a total area of 904.34 km^2. In the SE–NW direction, the ventilation conducive area was 728.80 km^2, accounting for 80.59% of the total area, which was higher than that in other directions. This direction was consistent with the dominant wind direction in Wuhan, indicating that the urban form of Wuhan is suitable for the wind environment. (2) The Yangtze River, Han River, and East Lake are natural open space areas, which formed the main framework of the VCs. These areas connected the suburbs with the city center, enabling cold and humid air to penetrate the core area of the city.

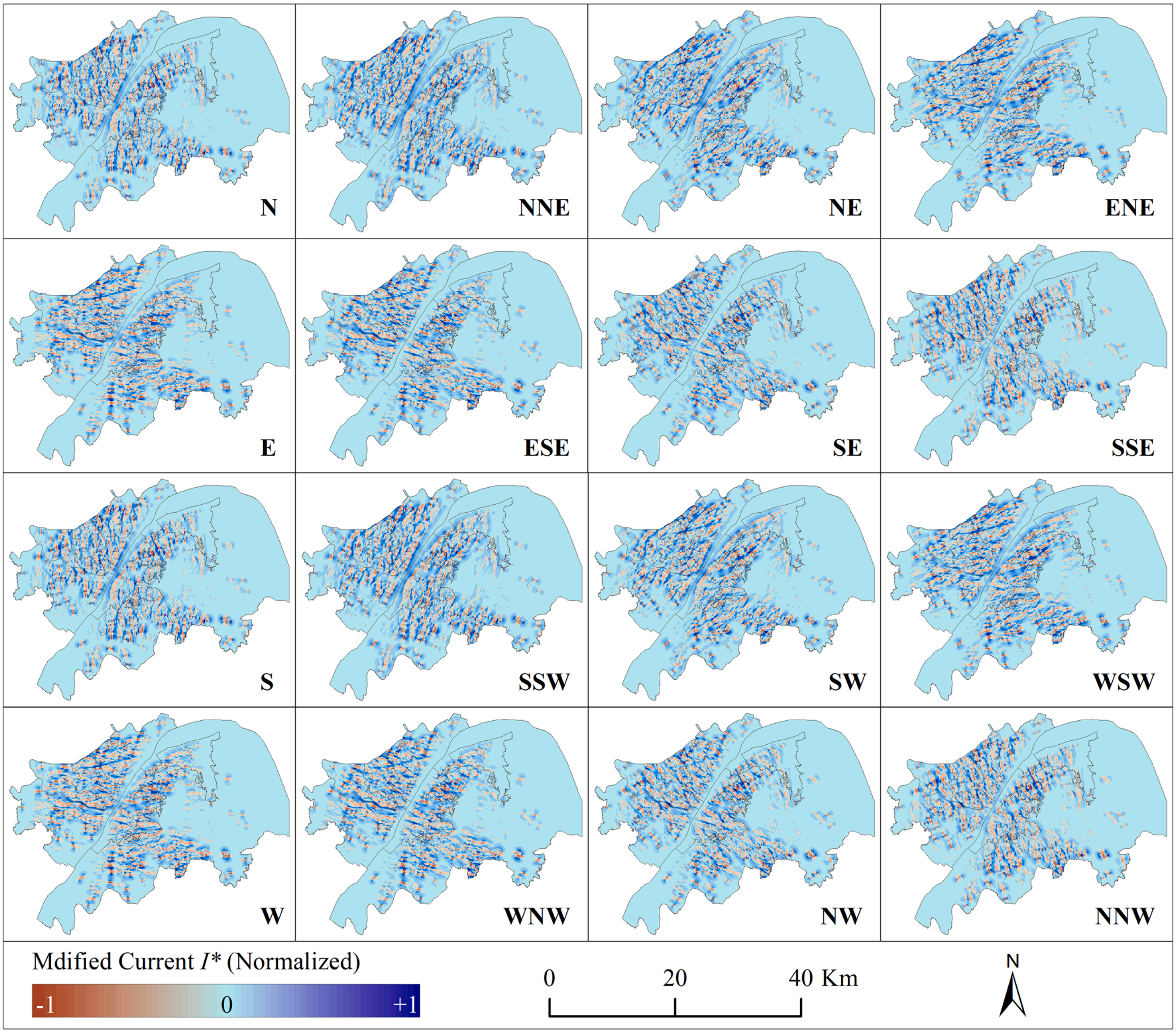

Fig. 10. Distribution map of VCs. Cell value represents the contribution of cell to ventilation. Blue indicates areas that promote ventilation, and red indicates areas that hinder ventilation.

Table 2
Statistical table of ventilation conducive area. Since most areas with the modified current value close to 0 were located in the suburbs, the area with $I^*\epsilon[-0.005,\ 0.005]$ was considered as ventilation conducive area.

Wind Direction	Hankou (Jianghan, Jiang'an, Qiaokou) Area (km^2)	Percentage (%)	Wuchan (Wuchan. Hongshan, Qingshan) Area (km^2)	Percentage (%)	Hanyang Area (km^2)	Percentage (%)
N	95.73	64.33	528.46	82.09	81.73	73.14
NNE	97.33	65.40	526.27	81.75	82.98	74.26
NE	101.12	67.95	542.93	84.33	87.10	77.95
ENE	96.04	64.54	532.49	82.71	82.32	73.67
E	98.82	66.40	543.77	84.46	85.63	76.64
ESE	99.97	67.18	543.70	84.45	85.78	76.77
SE	100.73	67.69	542.01	84.19	86.05	77.01
SSE	101.12	67.95	542.93	84.33	87.10	77.95
S	95.73	64.33	528.46	82.09	81.73	73.14
SSW	97.33	65.40	526.27	81.75	82.98	74.26
SW	101.12	67.95	542.93	84.33	87.10	77.95
WSW	96.04	64.54	532.49	82.71	82.32	73.67
W	98.82	66.40	543.77	84.46	85.63	76.64
WNW	99.97	67.18	543.70	84.45	85.78	76.77
NW	100.73	67.69	542.01	84.19	86.05	77.01
NNW	101.12	67.95	542.93	84.33	87.10	77.95

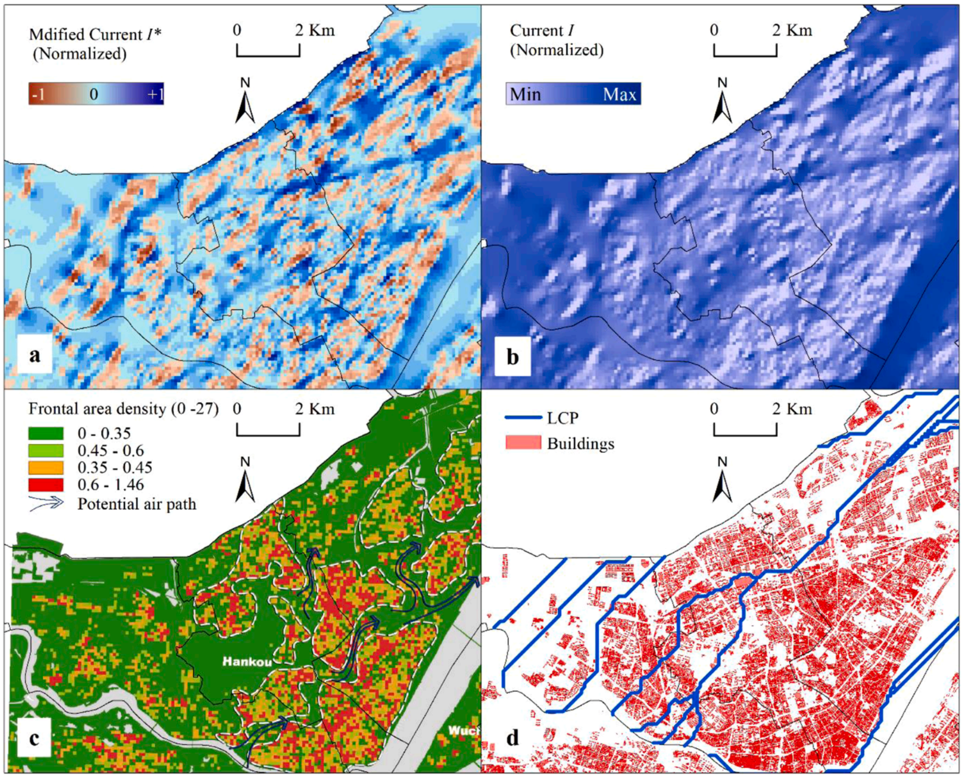

Fig. 11. VCs extracted using different methods: (a) NN—CM, (b) original current model, (c) rule-based model, and (d) LCP model.

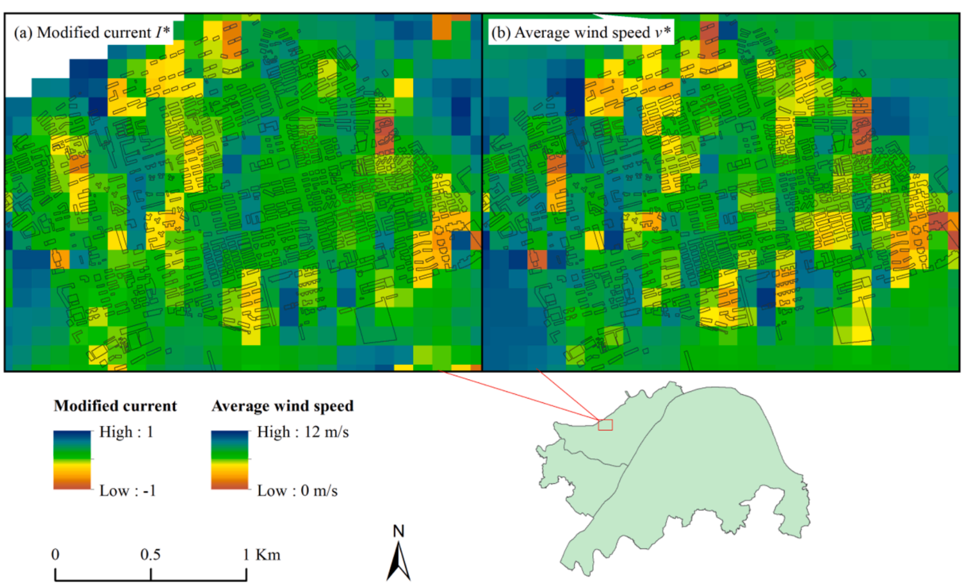

Fig. 12. Method verification based on CFD.

3)In the building up area, main roads formed long and narrow VCs. For example, the railway in the middle of Hankou and the second ring road in Qingshan District constituted the VCs in NE and SE directions, respectively.

An urban development strategy can be determined by combining the planning objectives with our analysis results. Hanyang and Wuchang are rich in natural open space resources. Complete utilization of the advantages of these resources is the basic strategy of VC construction in this area. Therefore, the protection of these water bodies should be strengthened by limiting the height and density of buildings around the water bodies. Hankou has a long history of development, resulting in less reservation of large natural open space. Fortunately, there are many small parks and lakes. During urban reformation, these small open spaces should be connected as much as possible. Further, constructing high-rise buildings between them should be avoided, particularly in the dominant wind direction.

4.4. Limitations

The proposed method exhibits certain limitations that should be considered during its application to address a given problem. The proposed method lacks rigorous hydrodynamic analysis, which is primarily reflected in three aspects. (1) FVI is a morphological index that uses the height profile of a three-dimensional building model in a certain area to express the ventilation capacity of the area. This generalization simplifies the complexity of the data and omits the basis of hydrodynamic analysis. (2) The sign of the corrected current value can better identify the boundary of the VC, but the mathematical relationship between its value and the ventilation volume still lacks strict data verification. (3) In the real world, the airflow in the urban canopy is affected by the friction of the ground and grounded objects, resulting in the loss of air kinetic energy. These hydrodynamic characteristics could not be effectively simulated and expressed using the method proposed in this study.

In this method, the neighborhood radius was set to a circular area of 1 km. Modifying this parameter can affect the calculation results. The selected value was effective for the case of Wuhan, as verified by the CFD test. However, when using this method to analyze other research areas, the value should be reasonably determined, and the calculated results should be verified by the CFD test to ensure the accuracy and effectiveness of the analysis.

As the ventilation volume in the VCs extracted by the proposed method lacks a quantitative description, further research should be conducted on VC scale sensitivity and flow quantification to further improve the accuracy of urban ventilation environment analysis.

5. Conclusion

In this study, an improved urban ventilation analysis method (NN—CM) was proposed. Considering the central urban area of Wuhan as the study area, the VCs in Wuhan were analyzed based on the three-dimensional building data in 2015 through a 100 m grid. The results demonstrated that this method could effectively identify the details of urban internal VCs and was suitable for wind environment analysis at the urban scale.

Compared with the wind tunnel, CFD, LCP-based, and rule-based urban VC simulation methods, NN—CM has advantages in data throughput, result coverage, and multi-wind direction dynamic simulation. Compared with the original urban VC analysis method based on the current model, NN—CM reduces subjectivity and improves the authenticity and reliability of the results. A case study in Wuhan verified the practical application of this method. Further, the study results demonstrated that the novel proposed method could help planners to integrate urban ventilation knowledge with urban planning parameters. Eqn. (1-5)

Declaration of Competing Interest

This manuscript has not been published or presented elsewhere in part or in entirety and is not under consideration by another journal. We have read and understood your journal's policies, and we believe that neither the manuscript nor the study violates any of these. There are no conflicts of interest to declare.

Acknowledgement

The authors would like to acknowledge all colleagues and friends who have voluntarily reviewed the translation of the survey and the manuscript of this study. This research study was supported by the National Natural Science Foundation of China (grant no. 41771178, 42030409, 41671151), the Shandong Province Natural Science Foundation Youth Branch (grant no. ZR2021QD078), the Fundamental Research Funds for the Central Universities (grant no. N2111003), Basic Scientific Research Project (Key Project) of the Education Department of Liaoning Province (grant no. LJKZ0964), Natural Science Foundation of Guizhou Province (grant no. [2019]1150), the Second Tibetan Plateau Scientific Expedition and Research Program (STEP) (grant no. 2019QZKK1004), and Innovative Talents Support Program of Liaoning Province (Grant No. LR2017017).

References

Chen, S. L., Lu, J., & Yu, W. W. (2017). A quantitative method to detect the ventilation paths in a mountainous urban city for urban planning: A case study in guizhou, China. *Indoor and Built Environment, 26*, 422–437. https://doi.org/10.1177/1420326X15626233

Chun, B., & Guldmann, J. M. (2018). Impact of greening on the urban heat island: Seasonal variations and mitigation strategies. *Computers, Environment and Urban Systems, 71*, 165–176. https://doi.org/10.1016/j.compenvurbsys.2018.05.006

Du, Y., & Mak, C. M. (2018). Improving pedestrian level low wind velocity environment in high-density cities: A general framework and case study. *Sustainable Cities and Society, 42*, 314–324. https://doi.org/10.1016/j.scs.2018.08.001

Gál, T., & Unger, J. (2009). Detection of ventilation paths using high-resolution roughness parameter mapping in a large urban area. *Building and Environment, 44*, 198–206. https://doi.org/10.1016/j.buildenv.2008.02.008

Gautam, K. R., Rong, L., Zhang, G., & Abkar, M. (2019). Comparison of analysis methods for wind-driven cross ventilation through large openings. *Building and Environment, 154*, 375–388. https://doi.org/10.1016/j.buildenv.2019.02.009

Gu, K., Fang, Y., Qian, Z., Sun, Z., & Wang, A. (2020). Spatial planning for urban ventilation corridors by urban climatology. *Ecosystem Health and Sustainability, 6*. https://doi.org/10.1080/20964129.2020.1747946

He, X., Li, Y., Wang, X., Chen, L., Yu, B., Zhang, Y., et al. (2019). High-resolution dataset of urban canopy parameters for Beijing and its application to the integrated WRF/Urban modelling system. *Journal of Cleaner Production, 208*, 373–383. https://doi.org/10.1016/j.jclepro.2018.10.086

He, Y., Tablada, A., & Hien, N. (2018). Urban Climate Effects of non-uniform and orthogonal breezeway networks on pedestrian ventilation in Singapore ' s high-density urban environments. *Urban Climate., 24*, 460–484. https://doi.org/10.1016/j.uclim.2017.03.005

He, Y., Tablada, A., & Hien, N. (2019). A parametric study of angular road patterns on pedestrian ventilation in high-density urban areas. *Building and Environment, 151*, 251–267. https://doi.org/10.1016/j.buildenv.2019.01.047

Hsieh, C. M., & Huang, H. C. (2016). Mitigating urban heat islands: A method to identify potential wind corridor for cooling and ventilation. *Computers, Environment and Urban Systems, 57*, 130–143. https://doi.org/10.1016/j.compenvurbsys.2016.02.005

Kim, H., Gu, D., & Kim, H. Y. (2018). Effects of Urban Heat Island mitigation in various climate zones in the United States. *Sustainable Cities and Society, 41*, 841–852. https://doi.org/10.1016/j.scs.2018.06.021

Lan, Y., & Zhan, Q. (2017). How do urban buildings impact summer air temperature? The effects of building configurations in space and time. *Building and Environment, 125*, 88–98. https://doi.org/10.1016/j.buildenv.2017.08.046

Lee, K. Y., & Mak, C. M. (2021a). Effects of wind direction and building array arrangement on airflow and contaminant distributions in the central space of buildings. *Building and Environment, 205*, Article 108234. https://doi.org/10.1016/j.buildenv.2021.108234

Lee, K. Y., & Mak, C. M. (2021b). Effects of different wind directions on ventilation of surrounding areas of two generic building configurations in Hong Kong. *Indoor and Built Environment*. https://doi.org/10.1177/1420326X211016040

McRae, B. H., Dickson, B. G., Keitt, T. H., & Shah, V. B. (2008). Using circuit theory to model connectivity in ecology, evolution, and conservation. *Ecology, 89*, 2712–2724. https://doi.org/10.1890/07-1861.1

Mostafavi, F., Tahsildoost, M., & Zomorodian, Z. (2021). Energy efficiency and carbon emission in high-rise buildings: A review (2005-2020). *Building and Environment, 206*, Article 108329. https://doi.org/10.1016/j.buildenv.2021.108329

Qiao, Z., Wu, C., Zhao, D., Xu, X., Yang, J., Feng, L., et al. (2019). Determining the boundary and probability of surface urban heat island footprint based on a logistic model. *Remote Sensing, 11*, 1–20. https://doi.org/10.3390/rs11111368

Qiao, Z., Xu, X., Wu, F., Luo, W., Wang, F., Liu, L., et al. (2017). Urban ventilation network model: A case study of the core zone of capital function in Beijing metropolitan area. *Journal of Cleaner Production, 168*, 526–535. https://doi.org/10.1016/j.jclepro.2017.09.006

Ren, C., Cai, M., Li, X., Shi, Y., & See, L. (2020). Developing a rapid method for 3-dimensional urban morphology extraction using open-source data. *Sustainable Cities and Society, 53*. https://doi.org/10.1016/j.scs.2019.101962

Ren, C., Yang, R., Cheng, C., Xing, P., Fang, X., Zhang, S., et al. (2018). Creating breathing cities by adopting urban ventilation assessment and wind corridor plan–the implementation in Chinese cities. *Journal of Wind Engineering and Industrial Aerodynamics, 182*, 170–188.

Ren, Jiayi, Yang, Jun, Zhang, Yuqing, Xiao, Xiangming, Xia, Jianhong Cecilia, Li, Xueming, & Wang, Shaohua (2022). Exploring thermal comfort of urban buildings based on local climate zones. *Journal of Cleaner Production.* , Article 130744. https://doi.org/10.1016/j.jclepro.2022.130744. In press.

Wicht, M., Wicht, A., & Osińska-Skotak, K. (2017). Detection of ventilation corridors using a spatio-temporal approach aided by remote sensing data. *European Journal of Remote Sensing, 50*, 254–267. https://doi.org/10.1080/22797254.2017.1318672

Wong, M. S., & Nichol, J. E. (2013). Spatial variability of frontal area index and its relationship with urban heat island intensity. *International Journal of Remote Sensing, 34*, 885–896. https://doi.org/10.1080/01431161.2012.714509

Wong, M. S., Nichol, J. E., To, P. H., & Wang, J. (2010). A simple method for designation of urban ventilation corridors and its application to urban heat island analysis. *Building and Environment, 45*, 1880–1889. https://doi.org/10.1016/j.buildenv.2010.02.019

Xie, P., Liu, D., Liu, Y., & Liu, Y. (2020). A least cumulative ventilation cost method for urban ventilation environment analysis. *Complexity*, 2020. https://doi.org/10.1155/2020/9015923

Xie, P., Yang, J., Wang, H., Liu, Y., & Liu, Y. (2020). A New method of simulating urban ventilation corridors using circuit theory. *Sustainable Cities and Society, 59*. https://doi.org/10.1016/j.scs.2020.102162

Yang, F., Qian, F., & Lau, S. S. Y. (2013). Urban form and density as indicators for summertime outdoor ventilation potential: A case study on high-rise housing in Shanghai. *Building and Environment, 70*, 122–137. https://doi.org/10.1016/j.buildenv.2013.08.019

Yang, J., Jin, S., Xiao, X., Jin, C., Xia, J.(Cecilia), Li, X., et al. (2019a). Local climate zone ventilation and urban land surface temperatures: Towards a performance-based and wind-sensitive planning proposal in megacities. *Sustainable Cities and Society, 47*, Article 101487. https://doi.org/10.1016/j.scs.2019.101487

Yang, J., Ren, J., Sun, D., Xiao, X., Xia, J.(Cecilia), Li, X., et al. (2021a). Understanding land surface temperature impact factors based on local climate zones. *Sustainable Cities and Society, 69*. https://doi.org/10.1016/j.scs.2021.102818

Yang, J., Wang, Y., Xiao, X., Jin, C., Xia, J.(Cecilia), & Li, X. (2019b). Spatial differentiation of urban wind and thermal environment in different grid sizes. *Urban Climate*, 28. https://doi.org/10.1016/j.uclim.2019.100458

Yang, J., Wang, Y., Xiu, C., Xiao, X., Xia, J., & Jin, C. (2020a). Optimizing local climate zones to mitigate urban heat island effect in human settlements. *Journal of Cleaner Production, 275*, Article 123767. https://doi.org/10.1016/j.jclepro.2020.123767

Yang, J., Yang, Y., Sun, D., Jin, C., & Xiao, X. (2021b). Influence of urban morphological characteristics on thermal environment. *Sustainable Cities and Society, 72*. https://doi.org/10.1016/j.scs.2021.103045

Yang, J., Zhan, Y., Xiao, X., Xia, J. C., Sun, W., & Li, X. (2020b). Investigating the diversity of land surface temperature characteristics in different scale cities based on local climate zones. *Urban Climate, 34*, Article 100700. https://doi.org/10.1016/j.uclim.2020.100700

Yuan, C., Norford, L., Britter, R., & Ng, E. (2016). A modelling-mapping approach for fine-scale assessment of pedestrian-level wind in high-density cities. *Building and Environment, 97*, 152–165. https://doi.org/10.1016/j.buildenv.2015.12.006

Yuan, C., Ren, C., & Ng, E. (2014). GIS-based surface roughness evaluation in the urban planning system to improve the wind environment - A study in Wuhan. *China, Urban Climate, 10*, 585–593. https://doi.org/10.1016/j.uclim.2014.06.005

Zhang, L., Zhan, Q., & Lan, Y. (2018). Effects of the tree distribution and species on outdoor environment conditions in a hot summer and cold winter zone: A case study in Wuhan residential quarters. *Building and Environment, 130*, 27–39. https://doi.org/10.1016/j.buildenv.2017.12.014

Zou, Z., Yan, C., Yu, L., Jiang, X., Ding, J., Qin, L., et al. (2021). Impacts of land use/land cover types on interactions between urban heat island effects and heat waves. *Building and Environment, 204*, Article 108138. https://doi.org/10.1016/j.buildenv.2021.108138